Magnetic characterization of isolated candidate vertebrate magnetoreceptor cells

Stephan H.K. Eder[a,1], Hervé Cadiou[b,2], Airina Muhamad[b,3], Peter A. McNaughton[b], Joseph L. Kirschvink[c], and Michael Winklhofer[a,4]

[a]Department of Earth and Environmental Sciences, Ludwig-Maximilians-University Munich, D-80333 Munich, Germany; [b]Department of Pharmacology, University of Cambridge, Cambridge CB2 1PD, United Kingdom; and [c]Division of Geological and Planetary Sciences, California Institute of Technology, Pasadena, CA 91125

Edited by Dennis Kent, Rutgers University/LDEO, Palisades, NY, and approved June 8, 2012 (received for review April 4, 2012)

Over the past 50 y, behavioral experiments have produced a large body of evidence for the existence of a magnetic sense in a wide range of animals. However, the underlying sensory physiology remains poorly understood due to the elusiveness of the magnetosensory structures. Here we present an effective method for isolating and characterizing potential magnetite-based magnetoreceptor cells. In essence, a rotating magnetic field is employed to visually identify, within a dissociated tissue preparation, cells that contain magnetic material by their rotational behavior. As a tissue of choice, we selected trout olfactory epithelium that has been previously suggested to host candidate magnetoreceptor cells. We were able to reproducibly detect magnetic cells and to determine their magnetic dipole moment. The obtained values (4 to 100 fAm^2) greatly exceed previous estimates (0.5 fAm^2). The magnetism of the cells is due to a μm-sized intracellular structure of iron-rich crystals, most likely single-domain magnetite. In confocal reflectance imaging, these produce bright reflective spots close to the cell membrane. The magnetic inclusions are found to be firmly coupled to the cell membrane, enabling a direct transduction of mechanical stress produced by magnetic torque acting on the cellular dipole in situ. Our results show that the magnetically identified cells clearly meet the physical requirements for a magnetoreceptor capable of rapidly detecting small changes in the external magnetic field. This would also explain interference of ac powerline magnetic fields with magnetoreception, as reported in cattle.

animal migration | biomineralization | salmoniformes | microrheology

Following the early idea that migrating animals might orient and navigate by the Earth's magnetic field, a large number of behavioral experiments have unequivocally established the existence of a magnetic sense in animals (see ref. 1 for a review). Nonetheless, so far only little is known about the biophysical principles that allow animals to detect the comparably weak geomagnetic field (2). Two working hypotheses for magnetoreception pathways are considered physically viable: (i) biomineralized magnetite particles connected to mechanosensitive structures (3–5) and (ii) magnetically sensitive chemical reactions involving a short-lived radical pair intermediate state (6–8). Magnetoreception by electromagnetic induction is considered possible only in marine electrosensitive animals (9, 10).

Salmonids, as well as zebra fish (Cypriniformes), yellow fin tuna, and Mozambique tilapia (Perciformes), which all lack electroreceptors (11), have been found to use the local magnetic field as a directional cue (12, 13) or to respond to artificial magnetic field stimuli in conditioning experiments (14–17). Most significantly, Walker et al. (15) were able to detect magnetically responding units in electrophysiological recordings from the superficial ophthalmic branch (rosV) of the trigeminal nerve of rainbow trout (*Oncorhynchus mykiss*) and to trace the origin of some of these units back to the olfactory epithelium. The candidate magnetoreceptor cells in the olfactory sensory epithelium were suggested to contain conspicuous iron-rich crystalline inclusions (15) with magnetic properties consistent with single domain magnetite (18). Despite this progress towards identifying the structural basis of magnetite-based magnetoreception in vertebrates, a number of key problems remain to be solved.

First and foremost, a method to quickly identify candidate magnetoreceptor cells should be established. Once such cells can be reproducibly isolated, specific experiments can be designed to study the nature of the cells and to provide biophysical constraints on the functional behavior of the magnetic inclusions. Here we present an ex vivo approach to tackle the problem of identifying and characterizing magnetite-based candidate receptor cells. In essence, a magnetic-field rotating in the focal plane of a light microscope is used to specifically look for magnetic cells in a suspension of cells, obtained by gentle dissociation of a sensory epithelium tissue. Magnetic cells will rotate with a frequency equal to that of the external magnetic field if their magnetic inclusions are linked to the cell membrane or at a slower rate if the magnetic torque is transmitted by intracellular viscous drag. Studying the characteristic hydrodynamic response time of magnetic cells to a magnetic field, we can test if the magnetic inclusion has a mechanically strong connection to the cell membrane and at the same time determine the cellular dipole moment.

Results

Visual Detection of Candidate Cells. In order to identify magnetic-material containing cells, we exposed a dissociated trout olfactory epithelium preparation to a moderately strong external magnetic field (2 mT) rotating slowly (0.33 Hz) in the focal plane of the microscope. Using these conditions, we observed the rotation of rare objects within the preparation. The dissociation of a pair of olfactory rosettes yielded, on average, 10^4 single cells in suspension, of which between one and four were found to rotate synchronously with the magnetic field. This result was observed in more than 50 animals. The majority of the magnetic cells had an elongated shape with typical dimensions of 10 to 20 μm and aspect ratio of 1.6, as the one shown in Fig. 1*A*. Another interesting feature of these cells is that they all contained an opaque inclusion under transmitted light (Fig. 1*A*, red arrows), which was highly reflective when observed in reflective light dark field

Author contributions: S.H.E., H.C., P.A.M, J.L.K., and M.W. designed research; S.H.E., H.C., A.M., and M.W. performed research; M.W. analyzed data; M.W. wrote SI Text; and S.H.E., H.C., J.L.K., and M.W. wrote the paper.

The authors declare no conflict of interest.

This article is a PNAS Direct Submission.

[1]Present address: Institute for Biological and Medical Imaging, Helmholtz-Center Munich, D-85764 Neuherberg, Germany.

[2]Present address: Université de Strasbourg, Institut des Neurosciences Cellulaires et Intégratives (INCI), Centre National de la Recherche Scientifique, Unité Propre de Recherche 3212, F-67084 Strasbourg, France.

[3]Present address: Institute of Biological Sciences, Faculty of Science, University of Malaya, Lembah Pantai, 50603 Kuala Lumpur, Malaysia.

[4]To whom correspondence should be addressed. E-mail: michael@geophysik.uni-muenchen.de.

This article contains supporting information online at www.pnas.org/lookup/suppl/doi:10.1073/pnas.1205653109/-/DCSupplemental.

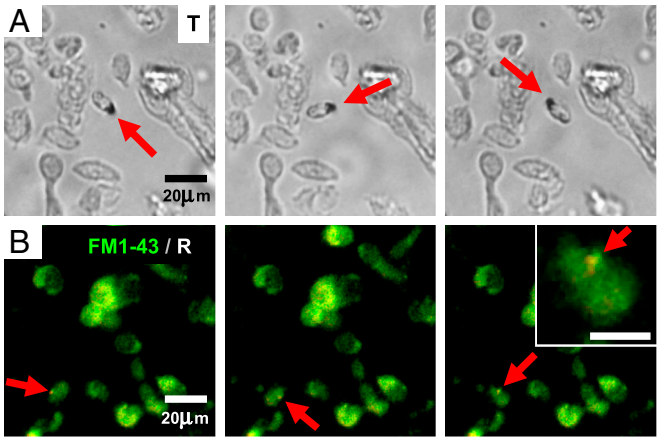

Fig. 1. Time lapses of cell suspension from dissociated trout olfactory epithelium, showing individual cells rotating with magnetic field. (See Movies S1 and S2 for the two full sequences from which time lapses were extracted). (*A*) Transmitted light (T), showing an opaque inclusion (red arrow) in the rotating object. (*B*) Simultaneously recorded dark-field reflection (R) and fluorescence (FM1-43, lipophillic dye), showing reflective objects (white) and cell membrane (green). The rotating cell contains a strongly reflective inclusion (red arrow), displayed as close-up (upper right corner, scale bar 10 µm).

(Fig. 1*B*, red arrows). In order to confirm the cellular nature of these rotating objects, we used the lipophilic dye FM 1-43fx, a marker already implemented for magnetotactic bacteria (19). A typical wide-field fluorescence image of a rotating cell stained with FM 1-43fx can be seen in Fig. 1*B*. (See Movies S1 and S2 for the full sequences from which Fig. 1*A* and *B* were extracted). The intracellular nature of the reflective objects was confirmed by confocal microscopy (Fig. 2). The opaque inclusions seen in the wide-field transmitted-light image (Fig. 2*A*) appear in confocal reflectance mode as brilliant elongated objects, with typical sizes of 1–2 µm (Fig. 2*B*). Under close inspection, these objects can be resolved into a structure of several reflective spots (see Fig. 2*B*, *Inset*). Significantly, the reflective objects are always found in the interior of the cell, well separated from the nucleus (see DAPI signal in Fig. 2*D*), but close to the cell membrane.

Intracellular Iron Detection. Some of the rotating cells were transferred onto clean glass slides in order to study the nature of the reflective objects (Fig. 3*A*, red arrow). Our working hypothesis

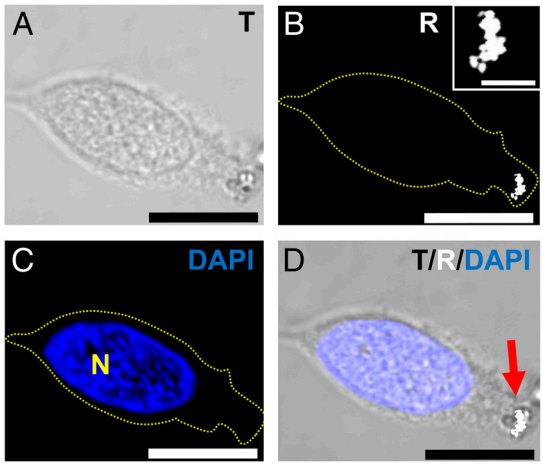

Fig. 2. Confocal images of candidate magnetoreceptor cell. (*A*) Transmitted light (T). (*B*) Same cell viewed in confocal reflectance mode (R). Dashed yellow line indicates cell outline. Reflective inclusions inside the cell, with a close-up view (upper right window, scale bar: 2 µm). (*C*) Confocal fluorescence image showing DAPI labeling of the same cell. N: nucleus. Dashed yellow line: cell outline. (*D*) Composite image showing the nucleus and the reflective inclusions (red arrow). Scale bar: 10 µm.

was that the reflective objects seen in light microscopy carry the magnetism of the cell. Therefore, it must be an iron-rich material because iron is the only element known to occur in biogenic magnetic minerals.

The transferred cell shown in Fig. 3 suffered a loss in integrity, giving us the opportunity to test whether the reflective object is strongly associated with the membrane or contained within the cytoplasm. As can be seen by comparing the reflected-light image (see *SI Text*) with the backscattered-electron image (Fig. 3*A*), the reflective object corresponds to the bright spot that strongly backscatters electrons. In contrast, no high-contrast feature is observable at that position in the secondary-electron image (Fig. 3*B*), which shows the surface properties of the sample. Since secondary electrons do not originate from deeper than 10 nm in a solid material, we can tell from the secondary-electron image (Fig. 3*B*) that the reflective object is a cellular inclusion and not an external contaminant that would otherwise be clearly visible as

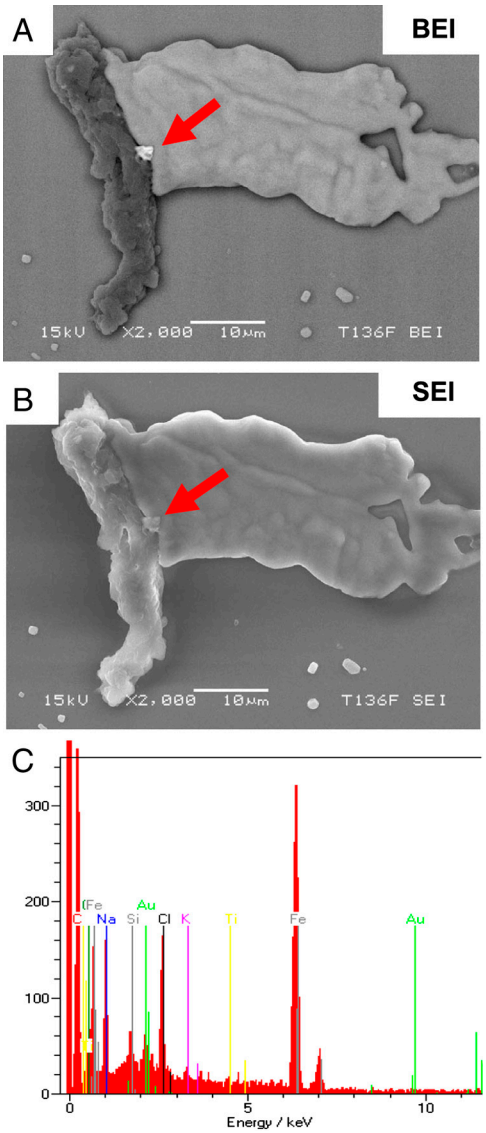

Fig. 3. Scanning electron microscopy of a previously rotating cell. Scale bars: 10 µm. (*A*) Backscattered electron image of the magnetic cell (left/vertical structure), which has lost cytoplasm (expelled to the right) during osmotic disintegration. The magnetic inclusion was retained (red arrow) and strongly backscatters electrons due to its high material contrast. (*B*) Secondary electron image does not reveal a contrast feature at the surface above the inclusion, demonstrating its intracellular nature. (*C*) Energy dispersive X-ray spectrum of the inclusion, showing a strong iron peak.

a high-contrast secondary-electron feature. Elemental analysis of the region containing the high-contrast backscattered-electron feature shows a strong iron peak (Fig. 3*C*), which was not seen outside that region. In contrast, the cytoplasm residue neither exhibited reflective objects nor had iron detectable by energy-dispersive X-ray analysis. The observation that the reflective object in the magnetically extracted cell corresponds to the iron rich, high-contrast backscattered-electron feature demonstrates that the reflective object is responsible for the magnetic properties of the cell. The magnetic inclusion most likely is mechanically anchored to the cell membrane rather than freely suspended in the cytoplasm because it remained in the cell after disruption rather than having been expelled with the cytoplasm.

Magnetic Characterization. The hypothesis that the magnetic inclusion has a mechanical connection to the cell membrane implies that the magnetic cell rotates at the same frequency as the driving frequency of the external magnetic field. Conversely, if the magnetic inclusion is only freely suspended in the cell, then there will be differential rotation between the cell membrane and the magnetic inclusion, as a consequence of which the cell will rotate at a distinctly slower rate (*SI Text*).

The cells were observed to rotate at the same frequency as the driving frequency of the external magnetic field. The time lapses displayed in Fig. 1*A* shows a $174 \pm 2°$ turn corresponding to 22 frames recorded at 15 fps, thus giving a frequency of 0.330 ± 0.003 Hz, which agrees with the driving frequency of 0.330 Hz. We did not observe any significant deviation between the driving and the cellular spinning frequency in any cell. From the absence of a frequency lag, we can conclude that the magnetic inclusions are directly coupled to the cell membrane rather than just viscously. This allows us to determine the magnetic dipole moment of the cells using the rotating field method (see *Materials and Methods*, *Theory*).

The magnetic dipole moment μ of $N = 13$ cells derived from eight animals is plotted as a function of the external magnetic field intensity H in Fig. 4. Most importantly, one can see that the magnetic moment is largely independent of the magnetic field strength over the field range covered here, which indicates that the cellular dipole moment is due to remanence-bearing—most likely single-domain—particles as opposed to superparamagnetic or multidomain particles, which would exhibit a pronounced

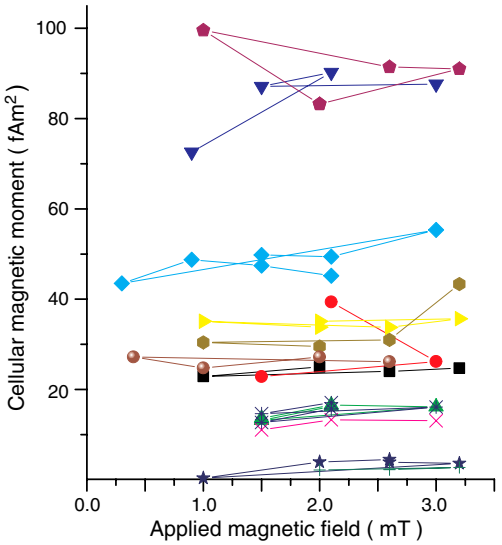

Fig. 4. Measured magnetic dipole moment μ as a function of the rotating magnetic field amplitude H for 13 cells. The individual $\mu(H)$ measurements for a given cell are connected according to the measurement sequence. See Table S1 for numerical values.

dependency of μ on H. Neither the fish nor the dissociated cells had been exposed to fields larger than 3 mT, which is below the switching fields required to remagnetize biogenic single-domain particles of magnetite in salmon (20–22). Hence, the measured magnetic dipole moments most likely reflect their natural values. It is possible that the original internal structure of the magnetic inclusion might not always have been conserved during sample preparation, in which case the natural cellular magnetic moment would be somewhat larger than the observed one.

Test for Cytoskeletal Connection of Magnetic Inclusion. The previous results have shown that the particle is located inside the cell (Figs. 2 and 3) and has a firm mechanical connection to the cell membrane. To specifically test whether the magnetic inclusions have a connection to the cytoskeleton, we used pharmaceutical agents, latrunculin B and colchicine, to specifically disrupt the cytoskeletal filaments F-actin and microtubules, respectively. If connected through these filaments to the cell membrane, the magnetic inclusion will become detached upon disruption, which then will result in differential rotation. We tested six cells with both drugs and found no decrease in the rotation rate of the magnetic cells relative to the driving frequency. From this observation, we conclude that these cytoskeletal filaments are not necessary for maintaining the mechanical connection of the magnetic inclusion to the cell membrane.

Discussion

We are able to unambiguously identify a cell as magnetic by its dynamic response to a rotating field. The method has three advantages in the search for candidate magnetite-based magnetoreceptor cells:

1. Detection of magnetic cells is highly specific, whereas other techniques based on iron detection (e.g., Prussian Blue staining of tissue sections) may give false positives, because not all biological iron compounds are (ferri)magnetic. Having used moderate magnetic field amplitudes, we can rule out false positives in the form of cells with inclusions of antiferromagnetic compounds [e.g., macrophages containing ferritin-like granules, siderosomes, and hemosiderin (23)], whose induced magnetization would become important only in much stronger magnetic fields. To achieve this goal, we accept false negatives represented by larger cells carrying a relatively low remanent magnetic moment, i.e., cells with magnetorotational mobility α much smaller than the f_B/B ratio we set when searching for spinning cells in suspension (*SI Text*). Usage of a stronger magnetic field (lower f_B/B ratio) is likely to increase the experimentally accessible range of magnetic cells towards low values of α but comes with the risk of obtaining false positives, which would then have to be sorted out using different methods. In such a case, a simple criterion for the presence or absence of magnetic remanence would be a field-flip test on a magnetic object in the suspension. A cell carrying magnetic remanence would rotate by 180°, whereas objects with induced magnetization would not. Further, we suggest the absence of distinct reflective particles in the visible cellular structure as a criterion for identifying false positives.
2. The method allows for a very sensitive measurement of the magnetic dipole moment of the cell, which is a key parameter in theoretical models of the receptor sensitivity threshold. The cellular magnetic dipole moments determined range from 4–100 fAm^2, which in a typical present-day Earth-strength magnetic field of 0.05 mT corresponds to a magnetic-to-thermal energy ratio $\mu \cdot B/kT$ of about 50:1 to 1,200:1 at physiological temperatures. These figures, on average, are significantly larger than those reported for most magnetotactic bacteria, which have magnetic moments of 0.2–1.7 fAm^2 (24–29). There are notable exceptions, however, such as *Magnetobacterium bavaricum* (10–60 fAm^2) (30, 31) as well as

some vibroid (8 fAm^2) (31) and some coccoid bacteria (2.4–54 fAm^2) (26).

Diebel et al. (18) used magnetic force microscopy (MFM) for detailed magnetic measurements on substructures of magnetic inclusions in an embedded trout olfactory epithelium. They obtained 0.5 fAm^2 ($\mu \cdot B/kT \sim 6$) for a group of crystals close to the scanned surface. The MFM technique is particularly sensitive to magnetic structures close to the surface of a tissue block but may underestimate the total magnetic moment of an intracellular inclusion dipping steeply away from the surface and extending 1 or 2 μm into the depth coordinate. The physical reason is the fast decay ($1/r^3$) of the magnetic stray field with distance from the magnetic source region. The rotating-field method in contrast quantifies the total magnetic moment of an individual cell.

Given that the cellular magnetic inclusions are made of single-domain magnetite (470 kA/m saturation magnetization) and assuming that all crystals are magnetized along the direction of the cellular magnetic dipole moment, just like in a bacterial magnetosome chain, our cellular magnetic moment values of 4–100 fAm^2 translate into a minimum magnetite volume of 0.01–0.2 μm^3 per cell. Taking typical crystal dimensions of about 50 nm (c.f. Fig. 2*a* in ref. 18), we obtain a minimum of 70–1,700 crystals per cell. It is clear that the crystals are not arranged in a linear chain, which would result in highly elongated inclusions exceeding the typically observed length of 1–2 μm, which also rules out a collapsed single-chain structure, as sometimes observed as a preparation artifact of magnetotactic bacteria (32). Rather, we suggest that the particles are arranged in the form of tightly packed bundles of chains, perhaps similar to the multistranded chains of magnetosomes described in *M. bavaricum* (31, 33, 34). It is important to note that crystals as small as 50 nm produce a pronounced reflection contrast under the confocal microscope, but the optical resolution limit of about 250 nm does not allow one to resolve the reflective spots seen in Fig. 2 into individual crystals. Each of these spots is likely to represent groups of crystals.

3. The method can be used to test whether magnetic inclusions are linked to the cell membrane, which is an important constraint when it comes to understanding the working principle and possible transduction pathway of magnetic signals in candidate magnetite-based magnetoreceptor cells (5). The fact that we observed an immediate mechanical reaction without differential rotation of candidate cells to a change in the external magnetic field implies that the magnetic torque acting on the magnetic inclusion is transmitted to the cell membrane through a mechanically strong connection rather than by mere viscous coupling across the cytoplasm. Actin filaments or microtubules do not appear to play a key role in the link because cells kept rotating after filament disruption. We hypothesize that the magnetic crystals are enclosed in a membrane structure contiguous with the cell membrane. This fits with our electron microscopy observations showing that inclusions are located close to the cell membrane.

A mechanically strong connection between magnetic dipole and cell membrane means transmission of stress without requiring motion of the magnetic inclusion, which avoids signal loss through viscous dissipation associated with motion. A number of theoretical models of magnetite-based magnetoreceptors assume rotational motion and conclude that viscous damping is too strong for the receptor to be susceptible to extremely low-frequency (50–60 Hz) magnetic fields due to ac powerlines (4, 35, 36). While this conclusion is theoretically sound, we find no evidence for rotational motion of the magnetic inclusion inside the cell, not even at 0.3 Hz. We therefore suggest that magnetic fields due to ac powerlines may well affect a magnetoreceptor with magnetic inclusions that are strongly mechanically coupled to the cell membrane. Interestingly, such fields have been reported to perturb the magnetic alignment behavior of artiodactyls and have been suggested to interfere with a magnetoreceptor (37, 38). Direct measurements of threshold sensitivity vs. frequency in honeybees (39) found a strong frequency drop-off and it is possible that magnetite-based Insect magnetoreceptors might have different cellular physiology.

In our proof-of-principle study, we focused on the olfactory epithelium of trout, which has been previously suggested to host candidate magnetoreceptor cells (15, 18). Ethmoid tissue (21, 40), lateral line (23), inner ear lagena receptors (41–43), corneal epithelium (44), and trigeminally innervated regions of the upper beak of birds (45) are other promising targets when searching for magnetic cells, which should be dispersed to avoid magnetostatic interactions.

In conclusion, we have introduced a new technique for isolating and characterizing candidate magnetite-based magnetoreceptor cells from dissociated tissue. We can reproducibly identify such cells under the microscope using a rotating magnetic field. By switching from transmitted light to reflected light in dark field, one can directly visualize highly reflective intracellular inclusions carrying the magnetism of the cell. Scanning electron microscopy demonstrated that iron-rich domains in magnetically isolated cells correspond to reflective objects under the light microscope. The measured magnetization curves of individual cells are consistent with single-domain magnetite. Surprisingly, the magnetic dipole moment of the candidate receptor cells is much larger than previously estimated and therefore not only sufficient to detect the direction of magnetic north but also likely to form the basis of an accurate magnetic sensory system with which to extract positional information from small spatial variations of geomagnetic field intensity and directions (46). The large magnetic moment also enables magnetoreception during times of low geomagnetic field strengths (47). Our observations indicate a firm connection between magnetic inclusion and cell membrane, which suggests an effective mechanism of transmitting the magnetic torque directly to stress-sensitive transducers without involving rotational motion and viscous damping. We believe that our technique has more control on the isolation of candidate cells than commercially available magnetic cell sorters and therefore sets the basis for a high-throughput method to collect cells for transcriptomic and proteomic analysis so as to study the molecular basis of magnetoreception and magnetite biomineralization.

Material and Methods

Theory. Consider a magnetic cell free to rotate in a suspension of cells. When exposed to an external magnetic field $\vec{B}(t)$ rotating at constant frequency f_B in the focal plane, a magnetic cell with permanent magnetic dipole moment $\vec{\mu}$ stiffly connected to the cell body will experience a magnetic torque $\vec{N}_{\text{mag}} = \vec{\mu} \times \vec{B}$ and a viscous resistance, $\vec{N}_{\text{vis}} = -\eta C \cdot \vec{\omega}$, where C is the tensor of frictional resistance coefficients for rotation in a viscous medium, η is the viscosity, and $\vec{\omega}$ is the instantaneous angular velocity of the cell. For a spherical cell with radius a, C is scalar and given by the well-known expression $C = 8\pi a^3$ (the components of C for ellipsoidal cells are treated in the *SI Text*). Introducing the rotation angle of the magnetic moment, $\theta(t) = \omega t - \psi$ with phase lag ψ, and the rotation angle of the magnetic field, $\varphi_B(t) = 2\pi f_B t$, where both are measured from the same point of reference in the focal plane, the torque balance can be written as

$$\mu B \sin(\varphi - \vartheta) = \eta C \frac{d\vartheta}{dt} \qquad [1]$$

Stationary solutions to this differential equation exist for a constant lag angle $\psi = (\varphi - \vartheta)$ between the magnetic moment and the magnetic field vector. Stationary conditions imply: $0 = d\psi/dt$, i.e., $0 = d\varphi/dt - d\vartheta/dt = 2\pi f_B - \omega$, i.e. $\omega = 2\pi f_B$, and Eq. **1** simplifies to

$$\frac{\mu B}{2\pi\eta C}\sin\psi = f_B \qquad [2]$$

The maximum frequency f_B of the external field (of a given intensity B) up to which the cell can rotate synchronously with the field (i.e., at $\omega = 2\pi f_B$) is given for a phase lag of $\psi = 90°$ and can be used to measure the magnetic dipole moment:

$$\mu = 2\pi\eta C\frac{f_B^{\max}}{B}, \qquad [3]$$

where $f_B^{\max}$ is also referred to as the boundary frequency (30). It is convenient to introduce the magnetorotational mobility α of a cell, i.e., $\alpha = \mu/(2\pi\eta C) = f_B^{\max}/B$, which is a constant for a cell dominated by remanent magnetization. If the ratio $f_B^{\max}$ to B increases with applied field strength, then the induced magnetization plays a role too, even though it is not the total induced magnetization, but only its anisotropic part that contributes to the torque. In the *SI Text*, it is shown that this anisotropic part of the induced magnetization leads to a B^2 dependency of $f_B^{\max}$ once the induced magnetization becomes larger than the remanent magnetization. To determine whether magnetization is due to remanence or to anisotropic magnetic susceptibility, we experimentally determined $f_B^{\max}$ for a range of B values for each cell.

Magnetoscope. To have precise control over the magnetic field in the focal plane, two orthogonal pairs of square coils were mounted around an inverted optical microscope (Zeiss ICM405 with Epiplan 40x, 0.85 N.A. Hellfeld/Dunkelfeld (HD), and 16x, 0.35 N.A. HD). The few magnetic parts of the microscope table were replaced by nonmagnetic ones to ensure a homogenous magnetic field within the sample plane. To rotate the magnetic field in the sample plane, the two coil pairs are fed with sinusoidal currents that have a constant phase shift of 90° relative to each other. The sinusoidal signals are generated by a two-channel arbitrary waveform generator (model M631, ETC, Slovak Rep.) and amplified with 400 Watt (50 V, 8 Amp) bipolar power supplies (Kepco Inc.).

Animals and Cell Isolation Procedure. Rainbow trout (length approximately 10 cm) were purchased from Mauka fish farm, Massenhausen, Germany and kept in a water circulating tank at 12 °C. Animals were killed in accordance with the German Animal Welfare Act (TierSchG). For animal killing, dissection, and cell isolation, iron-free nonmagnetic tools made of titanium, ceramics, and glass were used in order to avoid contamination with external iron present in standard lab tools. All tools and labware, if not presterilized, were cleaned in HCl or ethanol. Cell isolation was carried out as follows. After killing, olfactory rosettes were dissected out from both nasal cavities, using capsulotomy titanium scissors (Vannas), and placed in Ringer-1 solution on ice (containing100 mM NaCl, 3 mM KCl, 2 mM $CaCl_2$, 1 mM $MgCl_2$, 5 mM Hepes as buffer, 10 mM glucose, and adjusted to pH 7.4). All chemicals were of molecular biology grade (SigmaUltra) and buffers were made using Milli-Q water. For the dissociation of the olfactory epithelium, the rosettes were rinsed with Ringer-2 solution (without divalent cation salts, but otherwise identical to Ringer-1) and cut into millimeter-size pieces, followed by an incubation of 10 min in Ringer-2 solution under the presence of papain (Sigma; 0.25 mg/mL) activated with L-cystein (Sigma; 1.25 mg/mL), under constant stirring. After 10 min, the enzyme solution was removed and cells were washed twice with Ringer 2. The olfactory rosettes were then triturated gently using a fire polished Pasteur pipette tip. The dissociated cells were then centrifuged and the pellet resuspended in Ringer 1. Cells were left at 4 °C until use. The viscosity of Ringer-1 was measured with a concentric-cylinder viscometer (Brookfield Eng. Labs).

Identification and Extraction of Magnetic Cells. For detection of magnetic cells, a drop of the final cell suspension was placed on silanized coverslips (size 0, Menzel-Gläser). Silanization was achieved by adding chlorotributyl silane (Sigma-Aldrich) to glass coverslips and placing them in an oven at 150 °C for 20 min. This step was crucial in preventing cells from attaching to the glass surface. When searching for magnetic cells under the magnetoscope, we continuously rotated the magnetic field vector in the focal plane at a rotation frequency of $f_B = 0.33$ Hz and field intensity $B = 2$ mT (activating synchronous rotation of cells with $\alpha \geq 0.17$ mT^{-1} sec^{-1}; see *SI Text*) and systematically examined the suspension by scanning the preparation until a rotating cell was found. A field of 2 mT is low enough to avoid irreversible switching of single-domain particles. To determine the characteristic orientation time of a magnetic cell at a given external field strength B, we increased the field frequency f_B up to the point where the cell stopped rotating synchronously with the external field. Detailed magnetic measurements were performed on eight pairs of dissociated rosettes, which for this purpose were prepared in wet mounts with petroleum jelly seal to avoid desiccation-induced fluid motion (evaporation drift), which would otherwise produce additional force couples on the cells that are difficult to correct for in the theoretical treatment. In order to discriminate between cells and possible inorganic contaminants, we applied the lipophilic fluorescent dye FM 1-43fx (Invitrogen) at a final concentration of 5 μM in the sample solution. For extraction, magnetically identified cells in preparations without coverslip were collected by suction (CellTram vario, Eppendorf) with a microcapillary (FemoTips, Eppendorf) positioned with a joystick-controlled micromanipulator (PatchMan NP2; Eppendorf).

Image Processing. The snapshots shown in Fig. 1 of the paper have been extracted from Movies S1 and S2 in the *SI Text*, each recorded at 15 frames per second with a CCD camera (Chameleon, Point Grey Res.). All snapshots were despeckled with Image J software (National Institutes of Health (NIH)). In addition, the fluorescent images (Fig. 1*B*) were color-contrast balanced in image J.

Confocal Imaging. Dissociated olfactory cells were fixed using paraformaldehyde 4% in PBS with 0.2% glutaraldehyde, mounted with Vectashield hardmount mounting media containing DAPI, and sealed with coverslip. The settings of the confocal reflectance mode of the laser scanning microscope (Leica SP5 with DMI6000 B and x63 objective) were calibrated on magnetite chains in magnetotactic bacteria (15, 48), while *Escherichia coli* was used as negative control. Further analysis and image presentation were performed using Image J software (NIH).

Disruption of Cytoskeleton. For cytoskeleton disruption, dissociates containing spinning cells were observed for at least 30 min after treatment with latrunculin-B (Sigma L5288, final concentration 100 μM) against F-actin or colchicine (Sigma C9754, final concentration 500 μM) against microtubules, in concentrations high enough to disrupt the filaments (49) rather than to just stop them from polymerizing.

Scanning Electron Microscopic Analysis. Single cells were extracted and transferred to a coverslip with a grid to locate the cell after drying of the sample. Cells were plasma coated with gold and observed under a JSM5900LV (Jeol) at 15 kV. Elemental analysis was done with energy-dispersive X-ray spectroscopy at 15 kV (Röntec).

ACKNOWLEDGMENTS. We thank Marianne Hanzlik for assistance with electron microscopy and Valera Shcherbakov, Gil Westmeyer, and David Keays for discussions. This work was supported by the Human Frontier Science Organization (HFSP Grant RGP 28/2007 to J.L.K., P.A.M., and M.W.), Deutsche Forschungsgemeinschaft (DFG Grant Wi 1828/4-1 to M.W.), and the University of Malaya and Ministry of Higher Education Malaysia (to A.M.).

1. Wiltschko W, Wiltschko R (2005) Magnetic orientation and magnetoreception in birds and other animals. *J Comp Physiol A* 191:675–693.
2. Lohmann KJ (2010) Magnetic-field perception. *Nature* 464:1140–1142.
3. Kirschvink JL, Gould JL (1981) Biogenic magnetite as a basis for magnetic field detection in animals. *BioSystems* 13:181–201.
4. Kirschvink JL (1992) Comment on constraints on biological effects of weak extremely-low-frequency electromagnetic fields. *Phys Rev A* 46:2178–2186.
5. Winklhofer M, Kirschvink JL (2010) A quantitative assessment of torque-transducer models for magnetoreception. *J R Soc Interface* 7(Suppl 2):S273–289.
6. Schulten K, Swenberg CW, Weller A (1978) A biomagnetic sensory mechanism based on magnetic field modulated coherent electron spin motion. *Z Phys Chem NF* 111:1–5.
7. Rodgers CT, Hore PJ (2009) Chemical magnetoreception in birds: The radical pair mechanism. *Proc Natl Acad Sci USA* 106:353–360.
8. Ritz T, Ahmad M, Mouritsen H, Wiltschko R, Wiltschko W (2010) Photoreceptor-based magnetoreception: Optimal design of receptor molecules, cells, and neuronal processing. *J R Soc Interface* 7(Suppl 2):S135–146.
9. Paulin MG (1995) Electroreception and the compass sense of sharks. *J Theor Biol* 174:325–339.
10. Peters RC, Eeuwes L, Bretschneider F (2007) On the electrodetection threshold of aquatic vertebrates with ampullary or mucous gland electroreceptor organs. *Biol Rev* 82:361–73.
11. Albert JS, Crampton WGR (2005) Electroreception and electrogenesis. *The Physiology of Fishes*, ed D Evans (CRC, New York), 3rd Ed,, pp 429–470.
12. Quinn TP (1980) Evidence for celestial and magnetic compass orientation in lake migrating sockeye salmon fry. *J Comp Physiol A* 137:243–248.
13. Taylor PB (1986) Experimental evidence for geomagnetic orientation in juvenile salmon, *Oncorhynchus tschawytscha Walbaum. J Fish Biol* 28:607–623.
14. Walker MM (1984) Learned magnetic field discrimination in yellow fin tuna, *Thunnus albacares. J Comp Physiol A* 155:673–679.
15. Walker MM, Diebel CE, Haugh CV, Pankhurst PM, Montgomery JC (1997) Structure and function of the vertebrate magnetic sense. *Nature* 390:371–376.
16. Shcherbakov D, et al. (2005) Magnetosensation in zebrafish. *Curr Biol* 15:R161–162.
17. Hellinger J, Hoffmann KP (2009) Magnetic field perception in the rainbow trout, *Oncorhynchus mykiss. J Comp Physiol A* 195:873–879.
18. Diebel CE, Proksch R, Green CR, Neilson P, Walker MM (2000) Magnetite defines a vertebrate magnetoreceptor. *Nature* 406:299–302.
19. Keim CN, et al. (2004) Multicellular life cycle of magnetotactic prokaryotes. *FEMS Microbiol Lett* 240:203–208.
20. Kirschvink JL, Walker MM, Chang SBR, Dizon AE, Peterson KA (1985) Chains of single-domain magnetite particles in chinook salmon, *Oncorhynchus tshawytscha. J Comp Physiol A* 157:375–381.
21. Walker MM, Quinn TP, Kirschvink JL, Groot C (1988) Production of single-domain magnetite throughout life by sockeye salmon, *Oncorhynchus nerka. J Exp Biol* 140:51–63.
22. Moore A, Freake SM, Thomas IM (1990) Magnetic particles in the lateral line of the Atlantic salmon (*Salmo salar L.*). *Phil Trans R Soc Lond B* 329:11–15.
23. Treiber CD, et al. (2012) Clusters of iron-rich cells in the upper beak of pigeons are macrophages not magnetosensitive structures. *Nature* 484:367–370.
24. Frankel RB, Blakemore RP, Wulfe RS (1979) Magnetite in freshwater magnetotactic bacteria. *Science* 203:1355–1356.
25. Kalmijn AJ (1981) Biophysics of geomagnetic field detection. *IEEE Trans Magn* 17:1113–1124.
26. Esquivel DMS, Lins de Barros HGP (1986) Motion of magnetotactic microorganisms. *J Exp Biol* 121:153–163.
27. Winklhofer M, Abracado LG, Davila AF, Keim CN, Lins de Barros HGP (2007) Magnetic optimization in a multicellular magnetotactic organism. *Biophys J* 92:661–670.
28. Erglis K, et al. (2007) Dynamics of magnetotactic bacteria in a rotating magnetic field. *Biophys J* 93:1402–1412.
29. Pan YX, et al. (2010) Reduced efficiency of magnetotaxis in magnetotactic coccoid bacteria in higher than geomagnetic fields. *Biophys J* 97:986–991.
30. Steinberger B, Petersen N, Petermann H, Weiss D (1994) Movement of magnetic bacteria in time-varying magnetic fields. *J Fluid Mech* 213:189–211.
31. Hanzlik M, Winklhofer M, Petersen N (2002) Pulsed-field-remanence measurements on indivdual magnetotactic bacteria. *J Magn Magn Mater* 248:258–267.
32. Shcherbakov VP, Winklhofer M, Hanzlik M, Petersen N (1997) Elastic stability of chains of magnetosomes in magnetic bacteria. *Eur Biophys J* 26:319–326.
33. Hanzlik M, Winklhofer M, Petersen N (1996) Spatial arrangement of chains of magnetosomes in magnetotactic bacteria. *Earth Planet Sci Lett* 145:125–134.
34. Jogler C, et al. (2011) Conservation of proteobacterial magnetosome genes and structures in an uncultivated member of the deep-branching Nitrospira phylum. *Proc Natl Acad Sci USA* 108:1134–1139.
35. Adair RK (2000) Static and low-frequency magnetic field effects: Health risks and therapies. *Rep Prog Phys* 63:415–454.
36. Vanderstraeten J, Gillis P (2010) Theoretical evaluation of magnetoreception of power-frequency fields. *Bioelectromagnetics* 31:371–379.
37. Begall S, Cerveny J, Neef J, Vojtech O, Burda H (2008) Magnetic alignment in grazing and resting cattle and deer. *Proc Natl Acad Sci USA* 105:13451–13455.
38. Burda H, Begall S, Cerveny J, Neef J, Nemec P (2009) Extremely low-frequency electromagnetic fields disrupt magnetic alignment of ruminants. *Proc Natl Acad Sci USA* 106:5708–5713.
39. Kirschvink JL, Padmanabha S, Boyce CK, Oglesby J (1997) Measurement of the threshold sensitivity of honeybees to weak, extremely low frequency magnetic fields. *J Exp Biol* 200:1363–1368.
40. Mann S, Sparks NH, Walker MM, Kirschvink JL (1988) Ultrastructure, morphology and organization of biogenic magnetite from sockeye salmon, *Oncorhynchus nerka*: Implications for magnetoreception. *J Exp Biol* 140:35–49.
41. Harada Y, Taniguchi M, Namatame H, Iida A (2001) Magnetic materials in otoliths of bird and fish lagena and their function. *Acta Otolaryngol* 121:590–595.
42. Wu LQ, Dickman JD (2011) Magnetoreception in an avian brain in part mediated by inner ear lagena. *Curr Biol* 21:1–6.
43. Wu LQ, Dickman JD (2012) Neural correlates of a magnetic sense. *Science* 336:1054–1057.
44. Wenger RE, Begall S, Burda H (2006) Magnetic compass in the cornea: Local anesthesia impairs orientation in mammal. *J Exp Biol* 209:4747–4750.
45. Heyers D, Zapka M, Hoffmeister M, Wild JM, Mouritsen H (2010) Magnetic-field changes activate the trigeminal brainstem complex in a migratory bird. *Proc Natl Acad Sci USA* 107:9394–9399.
46. Lohmann KJ, Putman NF, Lohmann CMF (2008) Geomagnetic imprinting: A unifying hypothesis of long-distance natal homing in salmon and sea turtles. *Proc Natl Acad Sci USA* 105:19096–19101.
47. Kirschvink JL, Winklhofer M, Walker MM (2010) Biophysics of magnetic orientation: Strengthening the interface between theory and experimental design. *J R Soc Interface* 7(Suppl 2):S179–S191.
48. Green CR, Holloway H, Walker MM (2001) Detection of submicroscopic magnetite particles using reflectance mode confocal laser scanning microscopy. *Cell Biol Int* 25:985–990.
49. Woell S, Windoffer R, Leube RE (2005) Dissection of keratin dynamics: Different contributions of the actin and microtubule systems. *Eur J Cell Biol* 84:311–328.